Eur. Phys. J. B **17**, 253–259 (2000)

THE EUROPEAN PHYSICAL JOURNAL B

EDP Sciences

Mixing of wavefunctions in rectangular microwave billiards

U. Kuhl, E. Persson[a], M. Barth[b], and H.-J. Stöckmann

Fachbereich Physik, Philipps-Universität Marburg, Renthof 5, 35032 Marburg, Germany

Received 21 January 2000

Abstract. A set-up is described allowing the automatic registration of wavefunctions of quasi-two-dimensional microwave billiards of arbitrary shape. Tests of the apparatus with rectangular shaped billiards showed that a precision of some percent in the wavefunction amplitudes can be obtained, as far as isolated resonances are considered. For the case of overlapping resonances, however, the measurement yields wavefunctions which are close to a symmetric and an antisymmetric linear combination of the original rectangle eigenfunctions. The cause for this at first sight surprising result is discussed.

PACS. 03.65.Ge Solutions of wave equations: bound states – 41.20.-q Applied classical electromagnetism

1 Introduction

Ten years after the first experimental determination of the spectrum of a chaotic microwave billiard [1], analogue techniques have become a standard tool to study wave chaos in different types of chaotic resonators (see Chap. 2 of Ref. [2] for a review). In flat microwave resonators, in particular, there is a one-to-one correspondence between the Helmholtz equation and the stationary Schrödinger equation, including the boundary conditions. This allows an experimental approach to the study of questions related to quantum chaos. While most of the studies concentrated on the spectra of chaotic billiards and their interpretation in terms of random matrix theory or periodic orbit theory, there is an increasing number of publications aiming on the study of wavefunctions as well. Questions of interest were (i) the interpretation of wavefunctions in terms of classical trajectories, including the scarring phenomenon [3,4], (ii) an experimental realization of Berry's phase in triangular billiards [5], (iii) a demonstration of the fact that "you cannot hear the shape of a drum" [6], (iv) amplitude distribution functions in billiards with [7] and without [8] time-reversal symmetry, (v) chaos-assisted tunneling in annular billiards [9], and (vi) the localization - delocalization transition in disordered systems [7,10]. The localization of wavefunctions has been studied in one-dimensional disordered systems as well [11,12]. In one experiment field distributions in three-dimensional microwave resonators were studied [13]. The latter example differs from the previous ones in so far, as in three-dimensional electromagnetic systems the correspondence to the Schrödinger equation no longer holds.

In view of this increasing interest in wavefunctions in chaotic billiards and disordered systems we felt the need to automate the registration of wavefunctions. One of the topics of this paper is to describe the apparatus developed by us for this purpose. We shall concentrate on a test of the set-up with a rectangular billiard. The apparatus allows the registration of up to about 100 wavefunctions with a precision in the percent region. Problems arise only for the case of overlapping resonances. Here the measurement yield wavefunctions being close to a symmetric and an antisymmetric linear combination of the original wavefunctions. The interpretation of this result is the second topic of this paper.

Systems studied up to now were one Robnik billiard, also known as Pascal's limaçon [14], rough billiards [15], ray-splitting billiards, rectangular billiards with randomly distributed scatterers [10], and a system with topologically induced vortices [16]. As examples see the wavefunctions in Figure 1.

2 Experimental set-up

Figure 2 shows a sketch of the apparatus allowing an automatic registration of microwave billiard wavefunctions. The billiard consists of two parts made of brass: The upper part is a plate supporting an antenna in the centre. The antenna can be alternatively replaced by a metallic or dielectric cylinder allowing perturbing bead or level dynamics measurements as well [17]. The position of the top plate can be moved computer-controlled in x and y position in steps of 0.1 mm. The absolute precision of the positioning is, however, only of the order of 1 mm. The bottom part of the billiard can be moved up and down with help of a step motor. During the positioning

[a] *Present address:* Institute for Theoretical Physics, Vienna University of Technology, 1040 Vienna, Austria

[b] e-mail: michael.barth@physik.uni-marburg.de

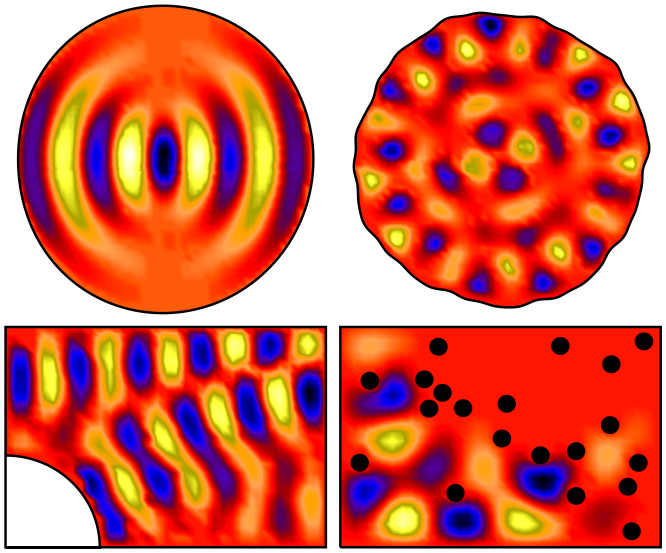

Fig. 1. Wavefunctions measured with the set-up described in Section 2. From top left to bottom right: Robnik billiard for $\lambda = 0.15$, rough billiard, ray-splitting billiard with a quarter circle teflon inset with $n = 1.44$, and disordered billiard with 20 circular metallic scatterers. The wavefunction amplitudes were converted into a grey scale with black corresponding to positive and white corresponding to negative signs. For more details see the references given in the text.

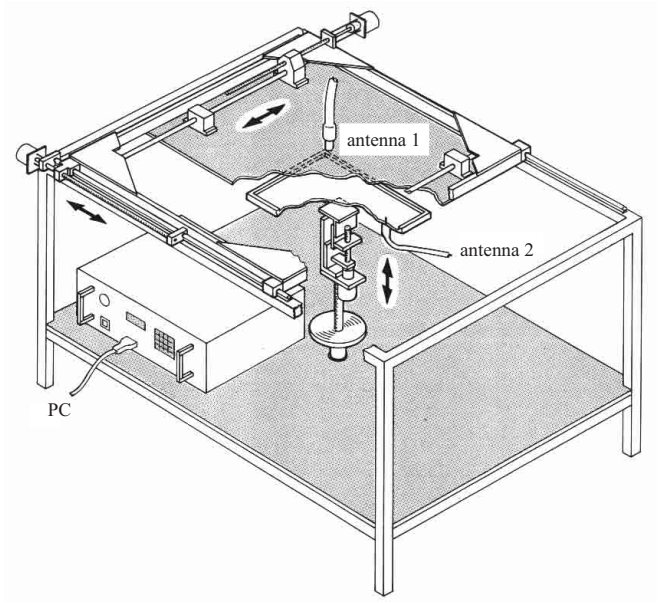

Fig. 2. Sketch of the apparatus. The height of the table is 75 cm, width and depth are 115 cm and 86 cm, respectively.

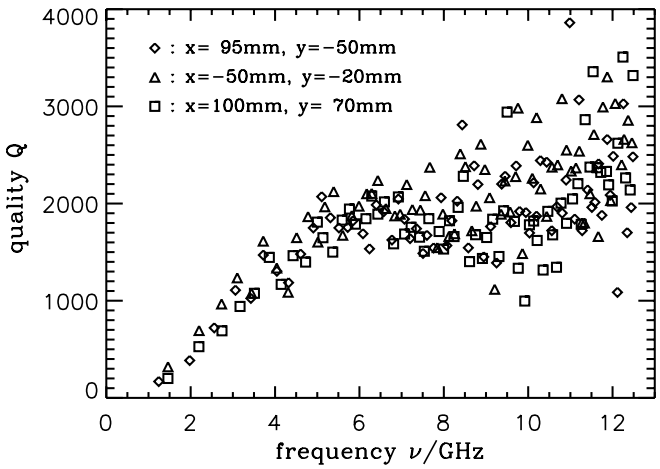

Fig. 3. Frequency dependence of the quality factor Q of the studied rectangular billiard. The different symbols refer to different antenna positions. For better visualization we only plotted every fifth resonance.

of the top plate the bottom part is lowered, during the measurement it is pressed towards the top plate. The bottom part of the billiard can easily be changed allowing the study of arbitrary shapes with a maximum size of 360×260 mm^2. The bottom part of the billiard may support a second antenna to allow transmission measurements as well. Each antenna consists of a small copper wire of diameter 0.3 mm attached to a standard SMA chassis connector and introduced through a small hole of diameter 1 mm into the resonator.

The number of resonances accessible to a mapping of wavefunctions is limited by the resonator quality given by $Q = \nu/\Delta\nu$, where ν is a given resonance frequency and $\Delta\nu$ its width. Figure 3 shows the experimental Q values in the frequency range 1 to 12 GHz. One observes an increase of Q with frequency up to about 5 GHz and a saturation at a Q value of about 2 000 for higher frequencies. Theoretically the Q value is given by

$$Q = \eta \frac{V}{\delta S} \tag{1}$$

where V, S are volume and surface of the resonator, and η is a geometrical factor of the order of one [18]. δ is the skin depth and is given in SI units as

$$\delta = \frac{1}{\sqrt{\pi \mu_0 \nu \sigma}} \tag{2}$$

where μ_0 is the vacuum permeability, and σ is the conductance of the wall material. From equations (1) and (2) one would expect a skin depth of 2 μm and a Q value of about 40 000 for $\nu = 5$ GHz, which is more than an order of magnitude larger as the experimentally observed value. The expected increase of Q with $\sqrt{\nu}$, too, is not found in the experiment. This shows that the quality is not limited by the skin depth but by small gaps between the bottom and the top part of the resonator, which cannot always be avoided, and which differ slightly for different positions. This only moderate Q value is the prize to be paid for the high flexibility of the apparatus. This limits the mapping of wave functions to about the 100 lowest eigenvalues. For the same reason a reliable determination of line widths is not possible with the set-up.

Usually the wavefunctions are registered with a resolution of 5 or 10 mm, corresponding to a total of about 2 000 spectra, each of it with 10 000 to 40 000 data points.

The frequencies were typically in the range 1 to 6 GHz. With the available Wiltron 360B vector network analyzer the time needed for a complete registration of about 100 wavefunctions amounted to about two weeks. With network analyzers presently available at the market this time can be reduced considerably.

3 Isolated resonances

The apparatus was tested with help of a rectangular billiard with side lengths $a = 340$ mm, $b = 240$ mm, and a height of $h = 8$ mm. A fixed antenna at the position $x = 80$ mm, $y = 20$ mm (measured from the centre of the rectangle) allowed the registration of transmission spectra as well. Thus all components S_{11}, S_{12}, S_{21}, S_{22} of the scattering matrix could be determined by the vector network analyzer. Scattering theory yields a relation between the scattering matrix S and the Green function G of the billiard [19],

$$S = \frac{1 - \imath W^\dagger G W}{1 + \imath W^\dagger G W}\,, \tag{3}$$

where the matrix W contains the coupling amplitudes w_{nj} of antenna j to eigenstate n. For the case of non-overlapping resonances equation (3) reduces to

$$S_{ij} = \delta_{ij} - 2\imath\gamma \sum_n \frac{\psi_n(r_i)\psi_n(r_j)}{k^2 - k_n^2 - \Delta_n + \imath\Gamma_n} \tag{4}$$

with shift and width of the resonances given by

$$\Delta_n = \Im(\gamma) \sum_j |\psi_n(r_j)|^2 \quad \text{and} \quad \Gamma_n = \Re(\gamma) \sum_j |\psi_n(r_j)|^2\,. \tag{5}$$

Here $\psi_n(r_j)$ is the value of the wavefunction at the position of antenna j. γ is a complex coupling constant depending on the antenna geometry. In equation (4) it is assumed that the antennas do not change the wavefunction ψ_n. This is justified in the limit, where the antenna radius is small compared to the wavelength and the eigenstates are not overlapping. See chapter 6 of reference [2] for a more detailed discussion of this point. For the case where two eigenstates are nearly degenerate, a more careful procedure is necessary as will be discussed in Section 4. From equation (4) it is evident that reflection spectra immediately yield $|\psi_n(r_j)|^2$ at the position of antenna j [4], whereas for the determination of the sign an additional transmission measurement is needed [19]. As an example Figure 4 shows $1-|S_{11}|$ in the range 2 to 2.3 GHz while the antenna was moved along the line $x = -50$ mm through the billiard. The maxima and the node lines of the wavefunctions are clearly discernible.

Close to an isolated resonance equation (4) reduces for the reflection measurement to

$$1 - S_{11} = \frac{b}{k^2 - c} \tag{6}$$

where $b = 2\imath\gamma\,|\psi_n(r_1)|^2$ and $c = k_n^2 + \Delta_n - \imath\Gamma_n$ are complex parameters. A fit with function (6) thus yields position, width and complex height of the resonances. One finally gets the quantity $\gamma\,|\psi_n(r_1)|^2$ as a function of position. Subsequently the constant γ is fixed by the normalization $\int |\psi_n(r)|^2\,\mathrm{d}A = 1$.

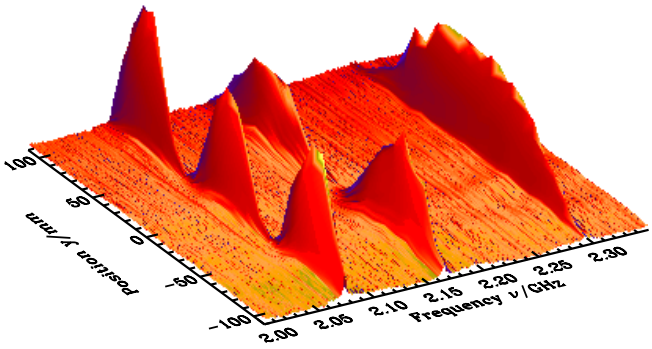

Fig. 4. Part of the spectra of a rectangular billiard ($a = 340$ mm, $b = 240$ mm). For a better visualization $1 - |S_{11}|$ is plotted, where S_{11} is the reflection amplitude at the movable antenna. The spectra were taken as a function of the y position of the antenna, with the x position fixed at $x = -50$ mm.

The sign of the wavefunctions is obtained from an additional transmission measurement. Just at the resonance position one obtains from equation (4)

$$S_{21}(r_2) = -2\gamma \frac{\psi_n(r_2)\psi_n(r_1)}{\Gamma_n} \tag{7}$$

with a complex prefactor. The phase of $S_{21}(r_2)$ jumps with π whenever the sign of $\psi_n(r_1)$ is changing and so can be used for detecting the sign of the wavefunctions. Figure 5 shows two such obtained wavefunctions for eigenfrequencies at 2.082 and 2.177 GHz, respectively (the two left resonances in Fig. 4). The left column shows the two wavefunctions in a grey scale where black corresponds to positive and white to negative signs. The middle column shows the phase of the transmission obtained from a measurement of S_{21} along the black lines shown in the left panel. For comparison the right column shows the calculated wavefunctions. The quality of the agreement can be judged from Figure 6, where calculated and experimental wavefunction amplitudes are plotted along a cut at $y = -30$ mm, for the same two wavefunctions as above. An overall agreement on a some percent level is found. A comparable good agreement between experiment and numerics was observed for the Robnik billiard [14].

4 Degenerate resonances

Due to the presence of the measuring antenna the resonances are shifted and broadened as is evident from equation (4). As a consequence the non-overlapping resonance approximation becomes obsolete in the moment where shifts and widths induced by the antennas and additional broadings due to the wall absorption are of the same order as the distance between the unperturbed resonances.

To see what happens we studied three pairs of close-lying resonances in more detail with unperturbed

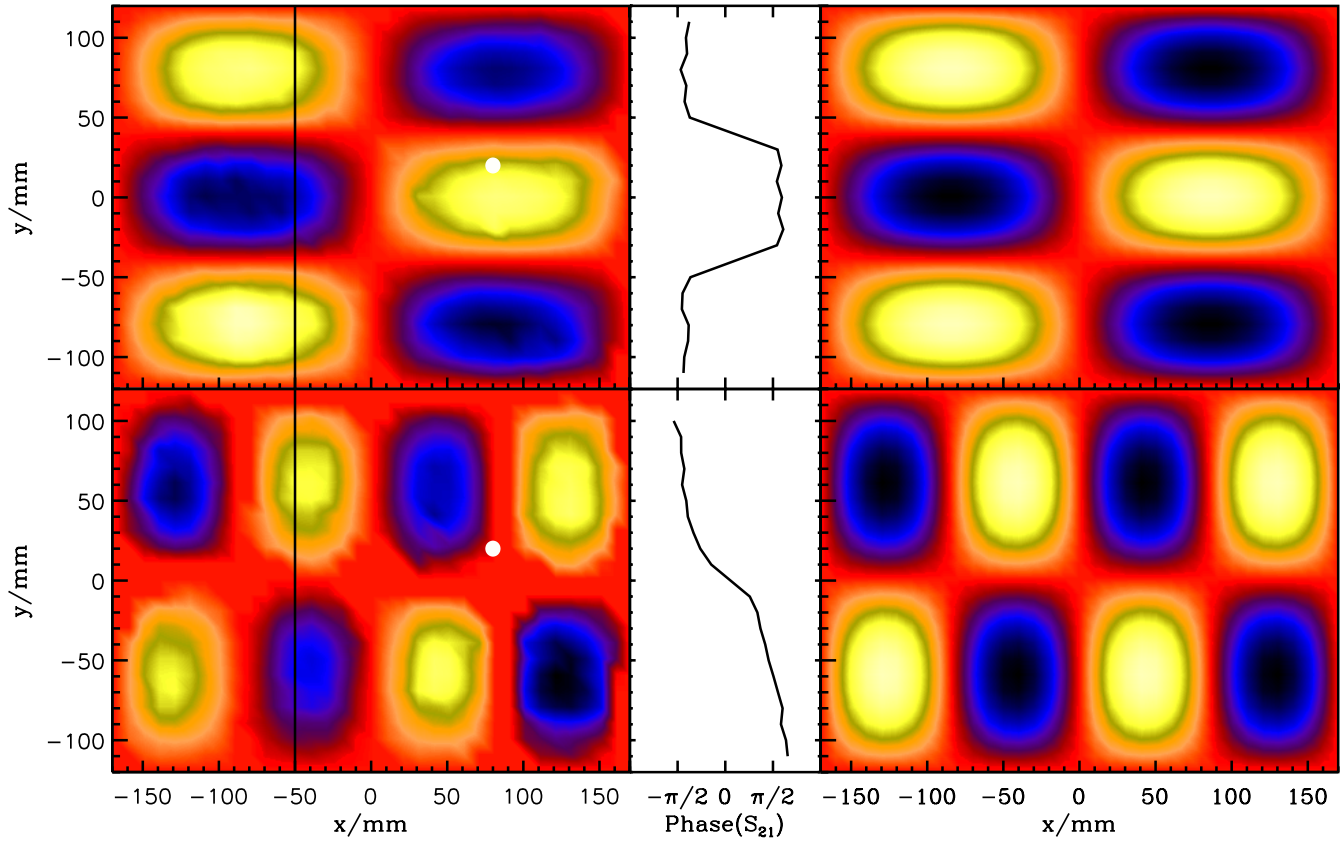

Fig. 5. Wavefunctions of the rectangle at eigenfrequencies 2.082 (top) and 2.177 (bottom) GHz. The left column shows the experimental amplitudes in a grey scale, the right column shows the theoretical expectation with the same resolution. In the middle column the phase of the transmission is plotted with one antenna moving along the black line in the left panel. The second antenna was fixed at the coordinates $x = 80$ mm, $y = 20$ mm (white dot in the left column, not in scale).

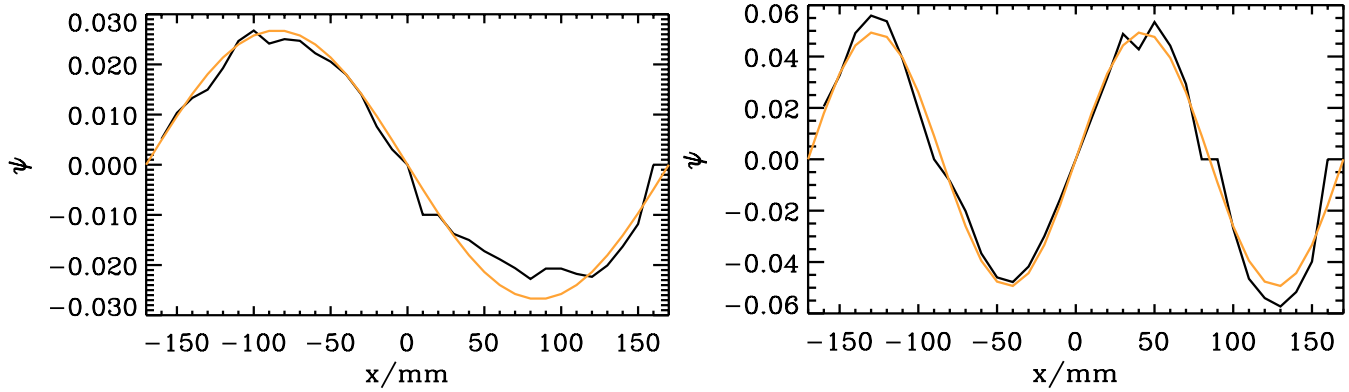

Fig. 6. Experimental (black) and theoretical (grey) wavefunction amplitudes for the same eigenfrequencies as in Figure 5, taken along the line $y = -30$ mm.

frequencies of 2.290/2.293 GHz (the right-most resonance structure in Fig. 4), 2.533/2.536 GHz, and 3.241/3.244 GHz. Fitting a superposition of two Lorentzians to the resonance lines, and associating the amplitude of the low-lying resonance with one wavefunction, and that of the high-lying resonance with the other one, the amplitude patterns shown in the left column of Figure 7 are obtained. In the right column the corresponding wavefunctions of the unperturbed rectangle are shown. The measurement did not yield the original wavefunctions, but patterns which are close to the symmetric and antisymmetric linear combinations.

Why are these findings surprising? Extending the calculation of the scattering matrix to the case of two overlapping resonances, it is easy to show that a data analysis as described above should always yield a linear combination

$$\begin{aligned} \psi_1 &= \psi_1^0 \cos\phi + \psi_2^0 \sin\phi \\ \psi_2 &= -\psi_1^0 \sin\phi + \psi_2^0 \cos\phi \end{aligned} \tag{8}$$

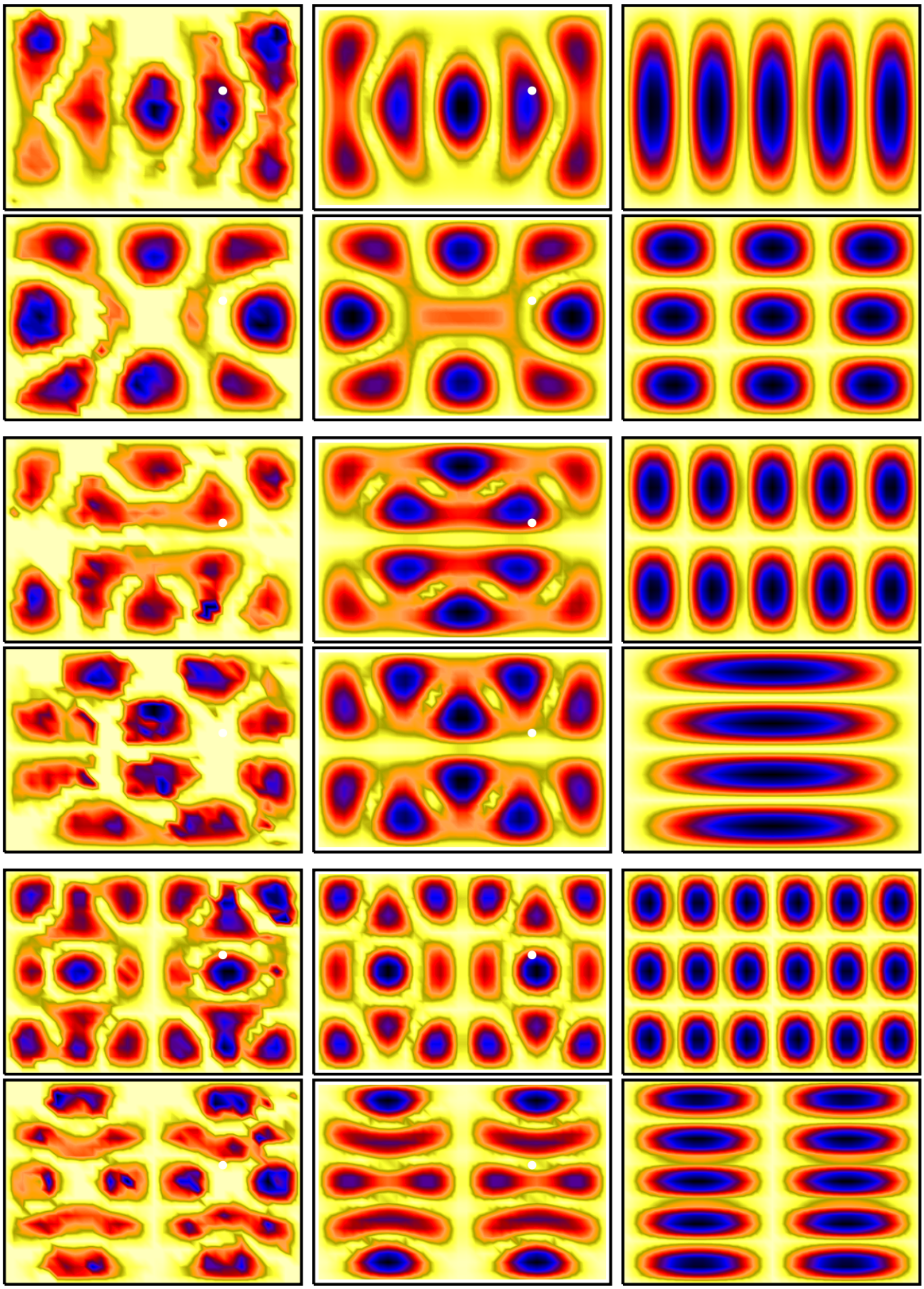

Fig. 7. Wavefunctions for three pairs of nearly degenerate resonances at the frequencies 2.290/2.293 GHz (top), 2.533/2.536 GHz (middle), 3.241/3.244 GHz (bottom). The left column shows the experimental results, in the right column the corresponding unperturbed eigenstates are shown. The middle column is the result of a simulation taking into account the influence of the fixed antenna, indicated by a white dot (not in scale).

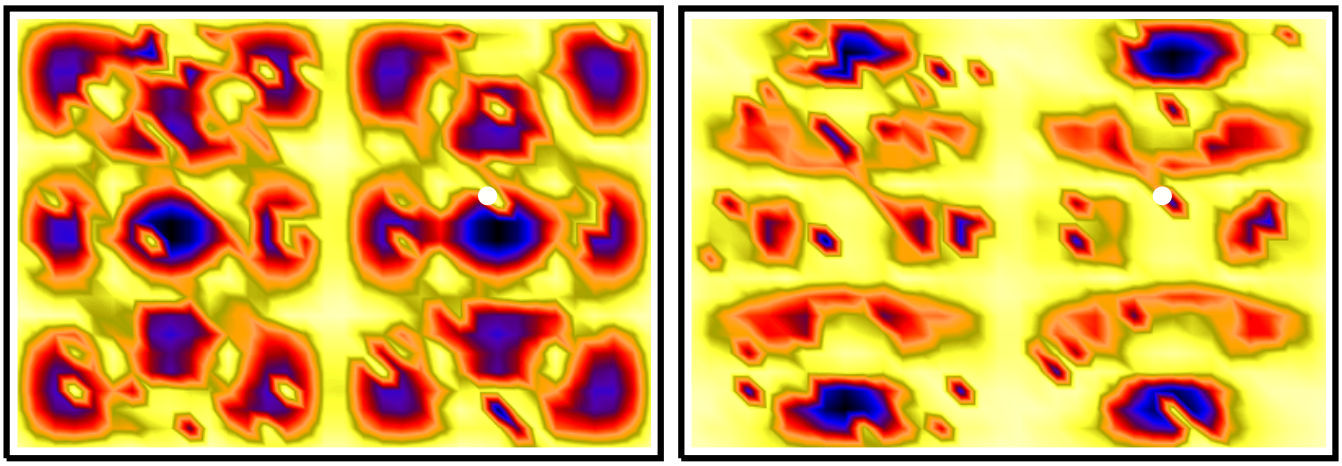

Fig. 8. Calculated wavefunctions for the bottom pair of resonances in Figure 7. Both the fixed and the movable antenna are taken into account.

of the original wavefunctions ψ_1^0, ψ_2^0. Thus fact of the mixing by itself is not astonishing. This explanation has, however, the draw-back that the mixing angle ϕ, too, is a function of the position of the moving antenna. In particular, there should be no mixing at all, if the antenna sits just on a node line of either resonance.

We therefore have to look for an additional mechanism locking the mixing angle. To get wavefunctions different from the original one, the separability of the x and y coordinates must be destroyed. There are three possible explanations, which shall be discussed now. We shall see that we can rule out all of them but one:

a) Wall absorption
The finite wall conductance causes a penetration of the electromagnetic wave into the walls by about 1 μm, as we have seen. It can be shown, that mixing angles due to the wall absorption are of the order of $(\delta/\lambda)^3$, where λ is the wavelength [20]. This is by far too small to explain the observed mixing. Even if we take into account that the observed Q values are by one order of magnitude smaller than theoretically expected, and express the reduced quality in terms of an effective skin depth, we end up with a value of about 3×10^{-5} mm for δ, still too small to explain the mixing.

b) Imperfections in the billiard fabrication
The billiards are manufactured with a precision of about 0.1 mm. To estimate the influence of the imperfections, we performed calculations, among others for a rectangle with an artificial surface roughness with an amplitude of 0.1 mm. The obtained mixtures were only in the percent region. Therefore mechanical imperfections, too, cannot account for the observed mixing.

c) Fixed antenna
It was stated above that for isolated resonances the influence of the antennas on the wavefunctions is negligible. This is no longer true for nearly degenerate resonances, and we shall see in a moment that the modification of the boundary conditions by the presence of the second fixed antenna is the very cause for the observed mixture of wavefunctions.

To understand the experimental findings, we simulated the cavity in the presence of antennas with a finite element method. The antennas were modeled by using outgoing wave boundary conditions,

$$\nabla_N E - \imath k E = 0 \,, \tag{9}$$

on the surface of the antennas. This implies ideal matching of the transmission line to the network analyzer. A more thorough treatment would take into account possible mismatches by correspondingly modified boundary conditions. This would complicate the calculations considerably and was not done, since a quantitative comparison with the experiment was not possible anyway for reasons to be discussed now.

In a first step, we calculated the resonances taking only the fixed antenna into account. The found mixing angle was very sensitive to the eigenfrequency spacing of the pairs. To get a large mixing of all the three pairs, a small adjustment of the size of the cavity was necessary. In the calculation we changed a by -0.2 mm and b by $+0.15$ mm, thus reducing the side ratio a/b by only 0.002, which is clearly within the production tolerance. By this the frequency spacing could be reduced for all three pairs simultaneously from 3 MHz to below 1 MHz.

The middle column of Figure 7 shows the such obtained wavefunction amplitudes. The overall agreement with the experimental data shown in the left column demonstrates that the fixed antenna alone is sufficient to reproduce the necessary mixing of the wavefunctions.

The question remains whether the agreement between simulation and experiment survives, if the moving antenna is considered as well. Since each position of the moving antenna corresponds to a new situation, altogether 759 different calculations had to be performed to obtain a single wavefunction. Figure 8 shows the results of the simulation for one pair of wavefunctions. The agreement between the simulation and the measurement is still good though the moving antenna has led to some modifications compared to the corresponding figures shown in Figure 7. The second antenna causes some extra mixing, but on average

the mixing remains around the value given by the fixed antenna. Similar results have been obtained for the two other pairs of wavefunctions.

As a résumé of this section it can be stated that the coupling of the cavity to the antennas noticeably disturbs the system, which leads to a mixing of the wavefunctions, if the states are almost degenerate. The mixing angle changes with the position of the moving antenna, but the presence of a fixed antenna leads to a locking of the mixing angle. Therefore the angle varies about an average given by the fixed antenna, but altogether the mixing remains fairly stable.

This work was supported by the Deutsche Forschungsgemeinschaft via the SFB 185 "Nichtlineare Dynamik". E.P. thanks the SFB 383 "Unordnung in Festkörpern auf mesoskopischen Skalen" for taking the costs for a three months stay in Marburg. Valuable discussions with I. Rotter, Dresden, and G. Veble, Maribor, are gratefully acknowledged.

References

1. H.-J. Stöckmann, J. Stein, Phys. Rev. Lett. **64**, 2215 (1990).
2. H.-J. Stöckmann, *Quantum Chaos - An Introduction* (Cambridge University Press, 1999).
3. S. Sridhar, Phys. Rev. Lett. **67**, 785 (1991).
4. J. Stein, H.-J. Stöckmann, Phys. Rev. Lett. **68**, 2867 (1992).
5. H.-M. Lauber, P. Weidenhammer, D. Dubbers, Phys. Rev. Lett. **72**, 1004 (1994).
6. S. Sridhar, A. Kudrolli, Phys. Rev. Lett. **72**, 2175 (1994).
7. A. Kudrolli, V. Kidambi, S. Sridhar, Phys. Rev. Lett. **75**, 822 (1995).
8. D.-H. Wu *et al.*, Phys. Rev. Lett. **81**, 2890 (1998).
9. C. Dembowski *et al.*, Phys. Rev. Lett. **84**, 867 (2000).
10. H.-J. Stöckmann *et al.*, Physica E (in press).
11. C. Dembowski *et al.*, Phys. Rev. E **60**, 3942 (1999).
12. U. Kuhl, H.-J. Stöckmann, Physica E (in press).
13. U. Dörr, H.-J. Stöckmann, M. Barth, U. Kuhl, Phys. Rev. Lett. **80**, 1030 (1998).
14. G. Veble *et al.*, Prog. Theor. Phys. Suppl. **139** (2000).
15. L. Sirko *et al.*, Phys. Lett. A **266**, 331 (2000); Y. Hlushchuk *et al.* (to be published).
16. P. Šeba, U. Kuhl, M. Barth, H.-J. Stöckmann, J. Phys. A **32**, 8225 (1999).
17. M. Barth, U. Kuhl, H.-J. Stöckmann, Phys. Rev. Lett. **82**, 2026 (1999).
18. J. D. Jackson, *Classical Electrodynamics* (Wiley, New York 1962).
19. J. Stein, H.-J. Stöckmann, U. Stoffregen, Phys. Rev. Lett. **75**, 53 (1995).
20. H.-J. Stöckmann (unpublished).